An X-ray Diffraction and Absorption Study of the Phases Formed upon Calcination of Zn−Al−Fe Hydrotalcites

I. Crespo,[†] C. Barriga,[†] M. A. Ulibarri,[†] G. González-Bandera,[‡] P. Malet,[‡] and V. Rives*,[§]

Departamento de Química Inorgánica e Ingeniería Química, Facultad de Ciencias, Universidad de Córdoba, Spain, Departamento de Química Inorgánica-Instituto de Ciencia de Materiales de Sevilla, Universidad de Sevilla-C.S.I.C., Sevilla, Spain, and Departamento de Química Inorgánica, Universidad de Salamanca, Salamanca, Spain

Received May 16, 2000. Revised Manuscript Received January 8, 2001

The thermal decomposition of hydrotalcite-like materials containing Zn(II), Fe(III), and Al(III) is studied. One of these samples contains zinc and aluminum in the brucite-like layers, while iron is incorporated as hexacyanoferrate(III) anions in the interlayer space. A second set of samples with Fe/Al atomic ratios in the range 0−1 contains zinc, iron, and aluminum cations in the layer and carbonate as the interlayer anion. When thermal decomposition is started from the latter precursors, X-ray diffraction only detects the formation of ZnO after calcination at 400−600 °C, while X-ray absorption spectra recorded at the Fe and Al−K absorption edges show that a fraction of trivalent cations migrates to tetrahedral holes in this temperature range. After calcination at 800 °C, the highest temperature achieved, two $ZnFe_yAl_{2-y}O_4$ spinels segregate, with a distribution of cations essentially normal, Fe/Al atomic ratios being different from the value of the starting material. On the other hand, thermal decomposition of the precursor that incorporates iron as hexacyanoferrate(III) yields already at 600 °C a mixture of ZnO and a single $ZnFe_yAl_{2-y}O_4$ spinel phase, whose Fe/Al atomic ratio coincides with the value of the original sample. Results suggest that the pyrolysis of the cyanide ligands at 400 °C leads to a coordination environment for iron highly disordered beyond the first-coordination shell, thus increasing the reactivity of iron and preventing the segregation of cations during the thermal decomposition of this sample.

Introduction

Hydrotalcite-like compounds, also called anionic clays or layered double hydroxides (LDH), have the formula $[M^{II}_{1-x}M^{III}_x(OH)_2](A^{n-})_{x/n}\cdot mH_2O$. Metallic cations are located in coplanar octahedra $[M(OH)_6]$ sharing edges and forming $M(OH)_2$ layers with the brucite (cadmium iodide-like) structure. The partial substitution of the divalent cations by trivalent ones involves a positive charge of the layer, balanced by anions between the hydroxylated layers, where water molecules also exist. A large number of LDHs have been synthesized,[1−4] changing the nature of trivalent and divalent cations in the layers or through intercalation of a great variety of anions between the brucite-like layers including simple inorganic anions (carbonate, nitrate, halides, etc.) and organic anions as well as complex anions and polyoxometalates.[5] In the same way, it is possible to synthesize LDHs containing three or more cations in the layers.

Decomposition of LDHs at moderate temperatures leads to mixed oxides of high specific surface area and reactivity that are of interest in catalytic applications. Thermal decomposition[2] starts at 200−300 °C and proceeds through amorphous phases, whose structure is not well-known. The final decomposition product is a mixture of $M^{II}M^{III}_2O_4$ spinel and $M^{II}O$ oxide because a M^{2+}/M^{3+} ratio above 1 is required to form a stable hydrotalcite and, therefore, the divalent cation is always in excess above the stoichiometry corresponding to the spinel. The first crystalline phase detected by X-ray diffraction (XRD) is usually MO,[2] while higher temperatures are needed to obtain diffraction peaks ascribed to the spinel and, therefore, XRD does not provide information about the state of trivalent cations at intermediate decomposition temperatures. Undetected trivalent cations are supposed[2] to be either forming amorphous phases (M_2O_3 or spinel-like) or substituting divalent cations in the MO phase because in some cases lattice parameters for the latter are slightly different from those reported for the bulk oxide. Studies of short range ordering in these materials using X-ray absorption spectroscopy (XAS) are useful for determining the

* To whom correspondence should be addressed. Fax: +34 923 294574. E-mail: vrives@gugu.usal.es.
[†] Universidad de Córdoba.
[‡] Universidad de Sevilla-C.S.I.C.
[§] Universidad de Salamanca.

(1) De Roy, A.; Forano, C.; El Malki, K.; Besse, J. P. In *Synthesis of Microporous Materials, vol. 2, Expanded Clays and other Microporous Systems*; Occelli, M. L., Robson, H. E., Eds.; Van Nostrand Reinhold: New York, 1992; p 108.
(2) Cavani, F.; Triffiro, F.; Vaccari, A. *Catal. Today* **1991**, *11*, 173.
(3) Triffiró, F.; Vaccari, A. In *Comprehensive Supramolecular Chemistry*; Atwood, J. L., MacNicol, D. D., Davies, J. E. D.; Vögtle, F., Lehn, J. M., Alberti, G., Bein, T., Eds.; Pergamon Press: Oxford, 1996; Vol. 7, p 251.
(4) Vaccari, A. *Catal. Today* **1998**, *41*, 53.
(5) Rives, V.; Ulibarri, M. A. *Coord. Chem. Rev.* **1999**, *181*, 61, and references therein.

10.1021/cm0010856 CCC: $20.00
Published on Web 04/06/2001

Table 1. Description of the Parent, Uncalcined Hydrotalcites

sample	formula[a]	Fe/Al[b]	Fe/(Fe + Al)[b]	Zn/(Fe + Al)[c]	a[d]	c[d]
ZAF-C-0.00	$[Zn_{0.74}Al_{0.26}(OH)_2](CO_3)_{0.13}\cdot 0.24H_2O$		0	2.88	3.077	22.86
ZAF-C-0.25	$[Zn_{0.73}Al_{0.22}Fe_{0.05}(OH)_2](CO_3)_{0.13}\cdot 0.46H_2O$	0.24	0.19	2.74	3.082	22.74
ZAF-C-0.50	$[Zn_{0.74}Al_{0.18}Fe_{0.09}(OH)_2](CO_3)_{0.13}\cdot 0.38H_2O$	0.51	0.34	2.78	3.090	22.82
ZAF-C-0.75	$[Zn_{0.73}Al_{0.16}Fe_{0.11}(OH)_2](CO_3)_{0.14}\cdot 0.33H_2O$	0.71	0.42	2.68	3.094	22.79
ZAF-C-1.00	$[Zn_{0.74}Al_{0.14}Fe_{0.12}(OH)_2](CO_3)_{0.13}\cdot 0.43H_2O$	0.90	0.47	2.89	3.095	22.85
ZA-F3	$[Zn_{0.66}Al_{0.35}(OH)_2](CO_3)_{0.13}[Fe(CN)_6]_{0.10}\cdot 0.74H_2O$	0.28	0.22	1.90	3.067	33.15

[a] Values have been rounded to two figures. [b] Global atomic ratio. [c] Atomic ratio for cations in the layers. [d] Å.

local order around these cations.[6−9] This technique provides information that effectively complements XRD data, yielding the local structure around cations both at the first-coordination shell (type of hole occupied) and second-coordination shell (metal−metal distances).

We have previously reported on hydrotalcite-like materials containing Zn(II) and Al(III) in the brucite-like layers and hexacyanoferrate in the interlayer,[10] where the effect of the synthesis route on the purity of the materials and the crystalline phases formed was analyzed as well as the effect on other materials with different Al/Fe ratios containing Zn(II), Al(III), and Fe(III) in the layers, but carbonate in the interlayer.[11] Previous studies[12] with Mg−Al−V hydrotalcites have shown that the original location of vanadium (as V^{3+} ions in the layer or as decavanadate in the interlayer) defines the nature of the phases formed upon calcination. In the present paper we report on the properties of the mixed oxides obtained after calcination of the Fe-containing materials mentioned above and on the effect of the initial state of iron ions (either in the layers or in the interlayer) on the nature and/or crystallinity of the phases formed.

Experimental Section

Synthesis of the Samples. A description of the precursor hydrotalcite samples studied is summarized in Table 1. Their synthesis has been described elsewhere.[10,11] Briefly, samples containing Zn(II), Al(III), and Fe(III) in the layers were prepared by dropwise addition of aqueous solutions of the nitrates with different starting atomic ratios (Zn/(Al + Fe) = 3 in all cases; Fe/Al = 0, 0.25, 0.50, 0.75, 1.0) into a beaker containing 100 mL of 1 M Na_2CO_3 aqueous solution with constant stirring (pH was kept constant to 10, using a 2 M NaOH aqueous solution). The precipitates were aged in the mother liquor at 65 °C for 3 h, centrifuged, washed and dried at 60 °C overnight, and calcined at selected temperatures for 2 h in air. Samples are named as ZAF-C-*X*-*T*, where *X* stands for the nominal Fe/Al atomic ratio and *T* for the calcination temperature (200, 400, 600, and 800 °C).

To prepare an additional sample containing hexacyanoferrate(III), a Zn(II),Al(III)-nitrate hydrotalcite precursor was prepared by dropwise addition of an aqueous solution of the nitrates with a Zn/Al atomic ratio of 2, to a boiled solution of NaOH (pH = 8.0), while nitrogen was continuously flowed to avoid carbonation from atmospheric CO_2. The solid thus obtained was filtered, washed, and suspended in decarbonated water, and a solution of hexacyanoferrate(III) was added (nominal Fe/Al ratio equal to 1.0); pH was maintained at 9.0 to avoid precipitation of the salt. The solid was aged for 24 h at room temperature, filtered, washed, then dried at 60 °C for 24 h, and then calcined at selected temperatures for 2 h in air. These samples are named as ZA-F3-*T*, where *T* stands for the calcination temperature, in °C (values as above).

Experimental Techniques. Powder X-ray diffraction (PXRD) patterns were recorded in a Siemens D-500 instrument, using Cu Kα radiation (λ = 1.54050 Å) and Al sample holders. In some diagrams diffraction lines due to Al are recorded and were used as a sort of internal reference to determine more precisely the positions of the diffraction peaks; the apparatus was equipped with AT Diffract software. Identification of the crystalline phases has been done by comparison with the JCPDS files (36-1451 for ZnO, 5-669 for $ZnAl_2O_4$, and 22-1012 for $ZnFe_2O_4$).

Thermogravimetric (TG) and differential thermal analyses (DTA) were carried out in TG-7 and DTA-7 instruments from Perkin-Elmer, in flowing oxygen (from L'Air Liquide, Spain), at a heating rate of 10 °C min^{-1}.

Room temperature X-ray absorption spectra (XAS) were obtained at the Daresbury SRS storage ring (Daresbury, UK). Data at the iron and zinc K-edges were recorded in transmission mode at station 7.1, using optimized ion chambers as detectors. Monochromatization was achieved with a double silicon crystal working at the (111) reflection, detuned 30% to reduce higher harmonics. Samples were mixed with boron nitride, using amounts previously calculated to get absorption coefficients close to 2.5, just above the absorption edge of interest, and edge jumps $\Delta\mu_x \sim 1$. Five scans were recorded and averaged to get final absorption spectra. XAS data at the aluminum K-edge were recorded at station 3.4 using the total electron yield detection method; samples were mixed with graphite and pressed into 13-mm-diameter disks. The EXAFS oscillations, $\chi(k)$, and the XANES data were obtained from the experimental XAS spectrum by conventional procedures.[13] Theoretical backscattering amplitude and phase shift functions for absorber-backscatterer pairs were calculated by using the program FEFF.[14] EXAFS data analysis and handling were performed by using the program package XDAP.[15] Different fit models were compared using the sum of the squares of the residuals between the fit and the data in *k*-space ($k^n - V$)[16]and/or the goodness of fit parameter (ϵ_ν^2).[17]

(6) del Arco, M.; Galiano, M. V. G.; Rives, V.; Trujillano, R.; Malet, P. *Inorg. Chem*. **1996**, *35*, 6362.
(7) del Arco, M.; Rives, V.; Trujillano, R.; Malet, P. *J. Mater. Chem*. **1996**, *6*, 1419.
(8) del Arco, M.; Malet, P.; Trujillano, R.; Rives, V. *Chem. Mater*. **1999**, *11*, 624.
(9) Bellotto, M.; Rebours, B.; Clause, O.; Lynch, J.; Bazin, D.; Elkaïm, E. *J. Phys. Chem*. **1996**, *100*, 8355.
(10) Crespo, I.; Barriga, C.; Rives, V.; Ulibarri, M. A. *Solid State Ionics* **1997**, *101−103*, 729.
(11) Barriga, C.; Kooli, F.; Rives, V.; Ulibarri, M. A. In *Synthesis of Porous Materials. Zeolites, Clays and Nanostructures*; Occelli, M. L., Kessler, H., Eds.; Marcel Dekker: New York, 1997; p 661.
(12) Kooli, F.; Crespo, I.; Barriga, C.; Ulibarri, M. A.; Rives, V. *J. Mater. Chem*. **1996**, *6*, 1199.
(13) Sayers, D. E.; Bunker, B. A. In *X-ray Absorption: Principles of EXAFS, SEXAFS and XANES*; Koningsberger, D. C., Prins, R., Eds.; Wiley: New York, 1988.
(14) Mustre de Leon, J.; Rehr, J. J.; Zabinsky, S. I.; Albers, R. C. *Phys. Rev. B* **1991**, *44*, 4146.
(15) A complete description of this program can be found in http://www.xs4all.nl.
(16) Percent variance values in *k*-space were defined as

$$k^n - V = 100 \times \int_{k_{min}}^{k_{max}} [k^n(\chi_{model}(k) - \chi_{exp}(k))]^2 dk / \int_{k_{min}}^{k_{max}} [k^n \chi_{exp}(k)]^2 dk$$

(17) Lytle, F. W.; Sayers, D. E.; Stern, E. A. *Physica B* **1989**, *158*, 701. The goodness of fit parameter is defined as

$$\epsilon_\nu^2 = \frac{\nu}{N_p(n - N_f)} \sum_{j=1}^{N_p} [\chi_{model,j} - \chi_{exp,j}]^2/\sigma^2$$

where N_p is the number of experimental data, N_f the number of free parameters, ν the number of degrees of freedom ($2\Delta k \times \Delta R/\pi + 1$), and σ the average error in experimental data, taken as 10^{-3}.

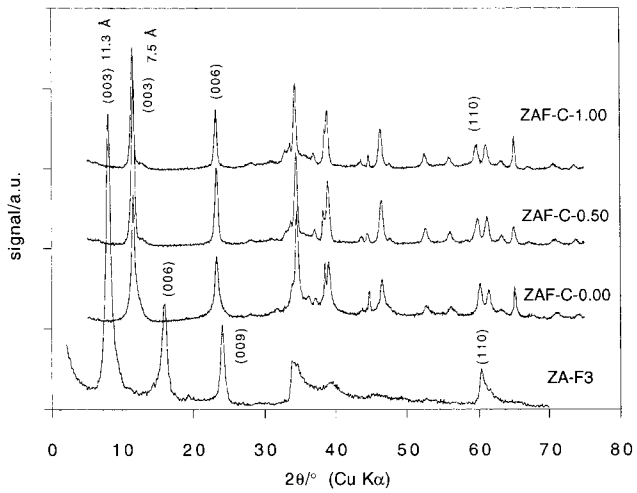

Figure 1. Powder X-ray diffraction patterns of precursor samples with the hydrotalcite-like structure. Patterns have been vertically displaced for clarity.

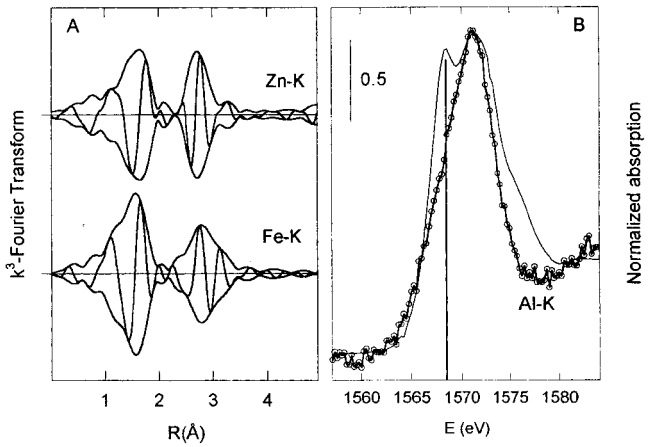

Figure 2. XAS data for the original ZAF-C-0.5 sample. (A) Modulus and imaginary part of the k^3-weighted Fourier transform of EXAFS oscillations at the Zn ($\Delta k = 2.4-13.6$ Å^{-1}) and Fe K-edges ($\Delta k = 2.5-11.1$ Å^{-1}). (B) XANES at the Al K-edge (−○−), data for boehmite (—) are included for comparison.

Results and Discussion

Precursors. All precursors showed X-ray diffraction patterns (see Figure 1) corresponding to well-crystallized hydrotalcites. Values for crystallographic parameters *c* and *a* are given in Table 1. According to a 3R stacking[18,19] of the sheets, the value of *c* is calculated as 3 times the spacing of the diffraction maximum corresponding to planes (003), while the value of *a* corresponds to the average metal−metal distance in the layers and is calculated as 2 times the spacing for planes (110).[2] Incorporation of Fe(III) in the layers gives rise to larger *a* values, in agreement with the larger ionic radius of Fe(III) than of Al(III);[20] the larger size of the hexacyanoferrate ion, in comparison to that of carbonate, accounts for the larger *c* value for sample ZA-F3. Thus, taking into account the thickness of the brucite-like layer (4.8 Å), carbonate-containing samples have gallery heights of 2.7−2.8 Å, while the gallery height for ZA-F3 is 6.2 Å. Both values are in agreement with the interlayer anions oriented with their C_3 axis perpendicular to the layers.[5,21]

X-ray absorption spectra (XAS) were recorded at Zn, Fe, and Al K-absorption edges. Because zinc and aluminum are located at the brucite-like sheets for all the precursors studied here, they show similar spectra at the Zn and Al K-absorption edges. Data obtained for ZAF-C-0.5 are included in Figure 2 as an example. Fourier transforms (FT) associated with EXAFS oscillations at the Zn−K edge show two maxima at 1.7 and 2.8 Å, as previously reported[6−8] for other transition metal cations in the layers of hydrotalcite samples. The first maximum is ascribed to oxygen atoms forming the first-coordination shell and best fit to our experimental data is achieved with 6.0−6.1 Zn−O distances at a shell radii, *R*, of 2.060 ± 0.02 Å. The second maximum is ascribed to M−M distances between [MO_6] octahedra that share edges in the brucite-like layers and yields M−M distances in the range 3.05−3.07 Å, in agreement with values for the *a* parameter determined by PXRD for the parent samples (3.062−3.088 Å). Al K-XANES for these precursors are characterized by a maximum at 1571 eV, with an ill-defined shoulder at its low-energy side. Peaks at 1568 and 1571−1572 eV are characteristic of compounds containing [AlO_6] octahedra[22] and, according to the expected octahedral coordination of aluminum cations in the layers, all features of Al K-XANES for the precursors appear at the same energies as those recorded for AlO(OH), boehmite (doublet with components close to 1568 and 1571 eV), a layered compound with edge-sharing [AlO_6] octahedra.[23]

As also shown in Figure 2 for ZAF-C-0.50, EXAFS data obtained at the Fe K-edge are similar to those recorded at the Zn K-edge for this precursor. Fe K-edge spectra for other ZAF-C-*X* samples are nearly identical because for these precursors iron cations are located in the brucite-like layers. Meanwhile, Figure 3 shows that EXAFS and XANES data at the Fe K-edge for ZA-F3 are almost identical to those recorded for crystalline K_3-[$Fe(CN)_6$], showing that the immediate environment of iron in hexacyanoferrate(III) remains almost unaltered when the anions enter the interlayer space. Coordination distances for Fe in bulk potassium hexacyanoferrate(III) are Fe−C 1.94 Å and Fe−N 3.08 Å.[24] According to the literature[25] the FT maximum close to 1.4 Å is ascribed to single scattering from the six nearest C neighbors, while the second maximum centered at 2.5 Å arises from single scattering by the six N neighbors and multiple scattering effects in the quasi-linear Fe−C−N chains. It should be noted that XANES features do not shift when going from $K_3[Fe(CN)_6]$ to anions intercalated in the hydrotalcite-like materials. In a previous paper we reported redox processes for hexacy-

(18) Bookin, A. S.; Cherkashin, V. I.; Drits, A. *Clays Clay Miner.* **1993**, *41*, 558.
(19) Bookin, A. S.; Drits, A. *Clays Clay Miner.* **1993**, *41*, 551.
(20) Huheey, J. E.; Keiter, E. A.; Keiter, R. L. *Inorganic Chemistry: Principles of Structure and Reactivity*, 4th ed.; Harper Collins College Publishers: New York, 1993.
(21) Drezdzon, M. A. *Inorg. Chem.* **1988**, *27*, 4628.
(22) Shimizu, K.; Kato, Y.; Yoshida, T.; Satsuma, A.; Hattori, T. *Chem. Commun.* **1999**, 1681.
(23) Wells, A. F. In *Structural Inorganic Chemistry*, 5th ed.; Oxford Science Publications: Oxford, 1984.
(24) Figgis, B. N.; Skelton, B. W.; White, A. H. *Aust. J. Chem.* **1978**, *31*, 1195.
(25) Westre, T. E.; Dicicco, A.; Filipponi, A.; Natoli, C. R.; Hedman, B.; Solomon E. I.; Hodgson, K. O. *J. Am. Chem. Soc.* **1995**, *117*, 1566.

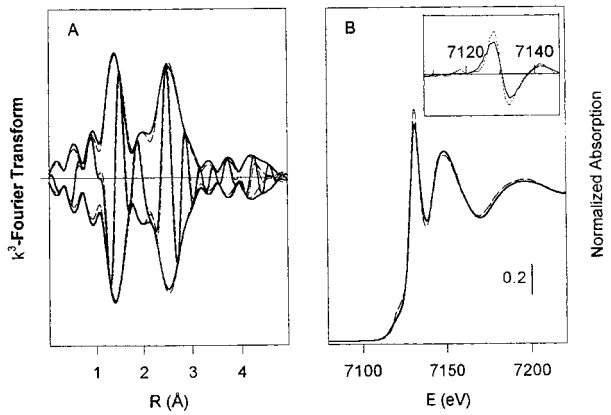

Figure 3. XAS data at the Fe K-edge for the original ZA-F3 sample (solid lines). Data for $K_3[Fe(CN)_6]$ (dashed lines) are included for comparison. (A) Modulus and imaginary part of the k^3-weighted Fourier transform of EXAFS oscillations ($\Delta k = 2.8-11.6$ Å^{-1}); (B) XANES; first-derivative absorption data are included as an inset.

anoferrates intercalated in Mg−Al LDHs,[26] in such a way that, whatever the synthesis started from solutions containing only hexacyanoferrate(II) or hexacyanoferrate(III), mixtures of both species were always obtained at the interlayer space. Differences between Fe−K edge XAS of $K_3[Fe(CN)_6]$ and $K_4[Fe(CN)_6]\cdot 3H_2O$ are detected at the near-edge region,[26] the absorption edge shifting 1 eV to lower energies when going from hexacyanoferrate(III) to hexacyanoferrate(II). Mixtures of both species give rise to a broadening of the intense XANES feature as well as to slight shifts in the main-edge position. None of these effects are observed for the ZA-F3 sample, and therefore a partial reduction of hexacyanoferrate(III) during intercalation seems to be absent in this case.

Thermal decomposition in air of samples containing interlayer carbonate has already been reported.[11] The curve for sample ZAF-C-1.00 is included in Figure 4A. Two endothermic peaks are recorded in the DTA profiles at ca. 137 and 228 °C, which, upon comparison with data for other hydrotalcites,[27] have been ascribed to removal of interlayer water molecules and decarbonation and dehydroxylation, respectively. For sample ZA-F3, Figure 4B, three weak endothermic peaks are recorded at 80, 196, and 310 °C, immediately followed by a strong exothermic peak at 420 °C ascribed[28] to pyrolysis of the cyanide ligands. It is important to note that above ca. 300 °C for samples ZAF-C and 500 °C for sample ZA-F3, no further thermal effects, nor any important weight loss, are recorded. Consequently, the parent hydrotalcite samples have been calcined in air for 2 h at 200, 400, 600, and 800 °C to identify the phases existing before or after each thermal effect or after high-temperature calcination, where crystallization of well-defined phases is expected.

Calcined Samples. PXRD patterns for calcined ZAF-C-*X* samples, $X = 0-1.00$, are rather similar and only those for Fe/Al = 1.0 are included in Figure 5. The layered structure is preserved at 200 °C, although basal lines slightly shift to *d*-spacings lower than those found

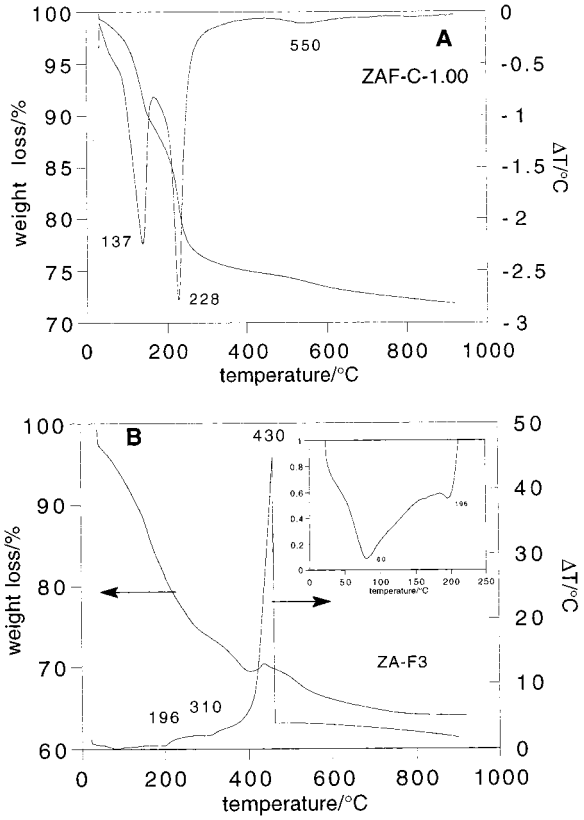

Figure 4. TG and DTA profiles for (A) ZAF-C-1.00 and (B) ZA-F3. The inset corresponds to the DTA profile of sample ZA-F3.

in the original sample, thus showing that the loss of water decreases the gallery height. After calcination at 400 °C basal lines have nearly vanished, indicating that the layered structure has been destroyed at this temperature, while broad diffraction lines characteristic of the zincite (ZnO) phase develop. Calcining at 600 °C increases the intensity and sharpness of the ZnO diffraction lines. Diffraction lines that could be ascribed to crystalline phases containing Fe(III) or Al(III) cations are absent for ZAF-C-400 and ZAF-C-600 and, therefore, the technique does not provide information about the location of trivalent cations in these samples. It should be noticed that diffraction lines ascribed to ZnO do not show any significant shift from the positions reported for the bulk material, expected if Al(III) and/or Fe(III) would have entered the ZnO lattice (Fe^{3+} and $A1^{3+}$ ionic radii are smaller than the Zn^{2+} ionic radius.[20]) However, calcination at 800 °C gives rise to sharp, well-defined peaks, which correspond to the presence of ZnO and a spinel, thus accounting for the presence of Fe(III) and/or Al(III) in the latter phase. It should be mentioned, however, that the ferrite-like spinel phase is detected mainly for the samples that have the higher Fe contents (vide infra). Identification of the precise spinels formed in ZAF-C-X-800 samples is difficult from PXRD results only. Some of the spinel diffraction maxima are fairly close to some diffraction maxima of ZnO. In our samples, because of the presence of iron, aluminum, and zinc, several $M^{2+}-M^{3+}$ combinations could be envisaged. Moreover, occupation by the different cations of tetrahedral and octahedral holes in the oxygen framework is not known a priori. Because ionic radii for Zn^{2+}, Fe^{2+}, Fe^{3+}, and Al^{3+} in tetrahedral coordination are 0.74, 0.77,

(26) Holgado, M. J.; Rives, V.; Sanromán, M. S.; Malet, P. *Solid State Ionics* **1996**, *92*, 273.
(27) Rives, V. *Inorg. Chem.* **1999**, *38*, 406.
(28) Miyata, S.; Hirose, T. *Clays Clay Miner.* **1978**, *26*, 441.

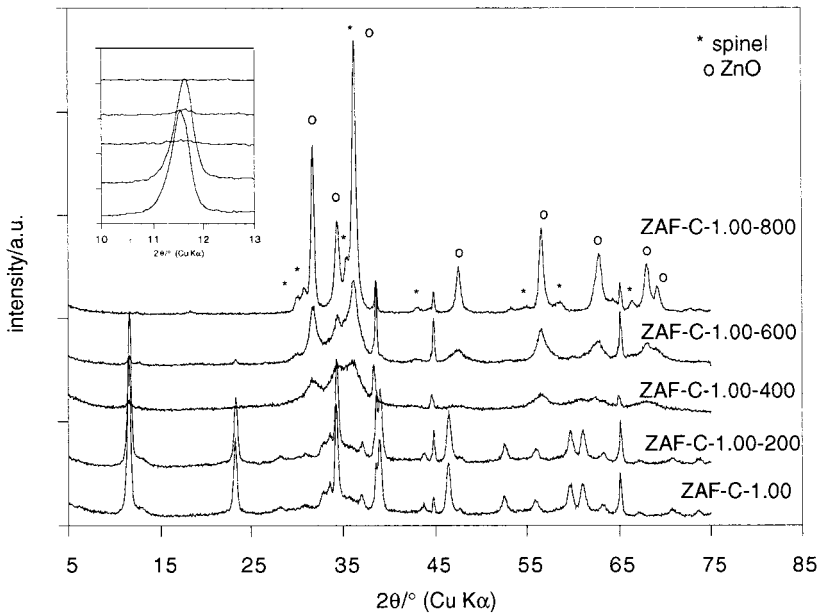

Figure 5. Powder X-ray diffraction patterns of ZAF-C-1.00-*T* samples. The inset shows the shift of the basal line at $2\theta = 11.5°$ after heating at 200 °C and how it vanishes after heating at higher temperatures. Patterns have been vertically displaced for clarity.

0.63, and 0.53 Å, respectively, while in high spin (where applicable) for octahedral coordination, they are 0.88, 0.92, 0.79, and 0.68 Å, respectively,[20] whichever the cations and the site occupancy in the lattice, diffraction peaks of spinel would be recorded in close positions. However, it should be noticed that spinel diffraction maxima recorded in our samples slightly shift and even split, depending on the starting precursor, thus suggesting changes in the composition and/or site occupancy of the spinel phase. More detailed conclusions about this point are reached below.

XAS provides information for the local environment of cations in the samples and experimental data recorded at Zn, Fe, and Al K-absorption edges were similar for ZAF-C-X-T samples with different *X* values, but calcined at the same temperature. As shown in Figure 6A for ZAF-C-1-*T*, the first-coordination shell FT maximum at the Zn K-edge slightly shifts to lower *R* values after thermal treatment at temperatures equal or higher than 400 °C. This change is accompanied by a shift of the second-shell maximum to higher *R* values and, in agreement with PXRD, Zn K-edge EXAFS spectra for samples calcined at $T \geq 400$ °C closely resemble that obtained for bulk ZnO. The best fit to experimental data indicates that four oxygen atoms form the first-coordination shell of zinc at 1.95−1.96 Å (Figure 6B). The simplest fit model considers that its second-coordination shell is formed only by Zn cations, yielding Zn−Zn shell radii 3.20−3.21 Å and, as also shown in Figure 6B, coordination numbers at this distance that increase as the calcination temperature does. Both Zn−O coordination parameters and Zn−Zn shell radii are characteristic of the ZnO phase, where zinc is in tetrahedral oxygen coordination and [ZnO_4] tetrahedra share a vertex to form the wurtzite-type structure. It is worth noting that the fit is not improved by including an additional Zn−Al shell close to 3.2 Å, accounting for aluminum substituting for zinc cations in the ZnO matrix. On the other hand, Zn K-edge EXAFS data of samples calcined at 800 °C show a

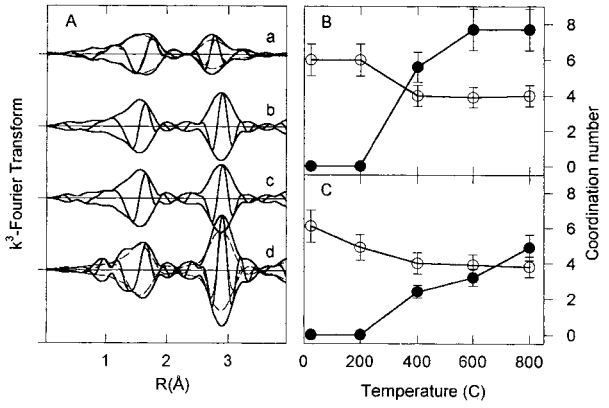

Figure 6. (A) k^3-weighted Fourier transform ($\Delta k = 2.4-13.6$ Å^{-1}) of EXAFS oscillations at the Zn K-edge for ZAF-C-0 calcined at (a) 200 °C, data for the precursor have been included as dashed lines; (b) 400 °C; (c) 600 °C; (d) 800 °C, data for crystalline ZnO have been included as dashed lines. (B) Coordination numbers for zinc obtained through best fit to EXAFS data for ZAF-C-0-*T*. (Open circles: first-coordination shell of oxygen atoms; fill circles: Zn neighbors at 3.2 Å); (C) Coordination numbers for zinc obtained through best fit to EXAFS data for ZA-F3-*T* (symbols as in B panel).

shoulder at the right-hand side of the second-shell FT maximum. This shoulder is absent for crystalline ZnO and can be ascribed to Zn−M distances arising from zinc cations that have entered the spinel phase detected by PXRD at this temperature. Actually, two Zn−M distances at 3.3−3.5 and 3.5−3.7 Å are expected from crystallographic data[29] for $ZnAl_{2-y}Fe_yO_4$ spinels ($0 \leq y \leq 2$), both of them being longer than the Zn−Zn distance found in ZnO. Fit to this shoulder was not attempted because it has a low intensity and includes two close Zn−M shell radii. It should be noted that the number of oxygen atoms at the first-coordination shell of zinc remains close to four after the detection of the spinel,

(29) Waerenborgh, J. C.; Figueiredo, M. O.; Cabral, J. M. P.; Pereira, L. C. J. *J. Solid State Chem.* **1994**, *111*, 300.

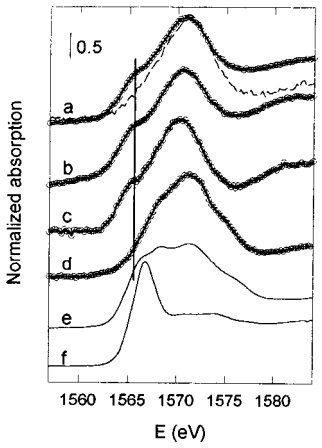

Figure 7. Al K-edge XANES for ZAF-C-0.5 calcined at (a) 200 °C, data for the precursor have been included as dashed lines; (b) 400 °C, (c) 600 °C, (d) 800 °C. Data for γ-Al_2O_3 (e) and $AlPO_4$ (f) have been included for comparison.

thus indicating that these cations occupy tetrahedral holes at the spinel phase as well.

Figure 7 includes Al K-XANES recorded for ZAF-C-0.5-*T* samples compared with data obtained for selected reference compounds. After calcination at 200−600 °C, in addition to the broad maximum detected for the precursor and ascribed to [AlO_6] units, a shoulder close to 1566 eV develops. According to the literature,[22] a white line peak at 1566 eV is characteristic of compounds containing [AlO_4] tetrahedra. Actually, the shoulder at low energies can be ascribed to [AlO_4] when the spectra for calcined samples are compared (see Figure 7) with those recorded for $AlPO_4$, a compound where Al cations are in tetrahedral oxygen coordination, and γ-Al_2O_3, where Al^{3+} distributes between octahedral and tetrahedral holes. As shown in Figure 7, these [AlO_4] units remain up to 600 °C and disappear after calcination at 800 °C. Similar results are obtained for ZAF-C-0-*T* and ZAF-C-1-*T* samples, thus indicating that aluminum cations in tetrahedral oxygen coordination are formed in ZAF-C-*X* samples calcined at moderate temperatures, most of them migrating to octahedral coordination sites at 800 °C.

Fe−K edge EXAFS data for ZAF-C-*X*-*T* samples after thermal treatments at 200−600 °C show (data for X = 1 are included in Figure 8A) an intensity of the first-shell FT maximum lower than that recorded for the original sample. Best fit to experimental data is achieved (Table 2) including two oxygen subshells at 1.87 and 2.02 Å, with coordination numbers 1.8−2.0 and 3.3−3.1, respectively.[30] When the calcination temperature is increased to 800 °C, the first-shell maximum recovers an intensity similar to that recorded for the parent sample and can be fitted by a single oxygen shell at 2.01 Å with coordination number 5.9. Results suggest that ca. 50% of iron cations migrate from octahedral holes in the brucite layers to tetrahedral holes when the sample is calcined at intermediate temperatures (200−600 °C), while all of them occupy octahedral holes after calcination at the highest temperature achieved (800 °C). It should be noted that, although PXRD and Zn K-edge EXAFS data reported above showed that the layered structure is preserved at 200 °C, a fraction of iron and aluminum cations already occupies tetrahedral holes at this temperature. This result shows, as previously reported for other systems,[8,9] that trivalent cations leave their positions in the brucite-like layers at the first stages of the thermal decomposition process. Near-edge region of the Fe K-spectra, shown in Figure 8B, confirms this model. Thus, although main XANES features for ZAF-C-1-*T* samples are similar to those previously reported for $Fe(NO_3)_3{\cdot}9H_2O$,[8] a compound where Fe(III) is in octahedral oxygen coordination, XANES data for samples calcined at 200−600 °C show increased intensities of the pre-edge feature, better seen in the first-derivative spectra, this intensity again decreasing after calcination at 800 °C. An increase in the intensity of the 1s → 3d pre-edge feature is expected when going from octahedral to tetrahedral coordination,[31] because of the loss of inversion symmetry at the iron site. It should be noted that neither the pre-edge peak nor the main edge shift their energy after calcination, remaining

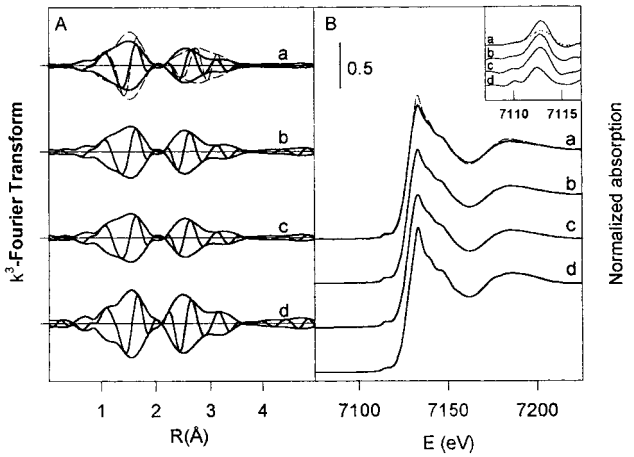

Figure 8. Fe K-edge XAS data for ZAF-C-1-*T*: (A) k^3-weighted Fourier transform of EXAFS oscillations (Δk = 2.5−11.1 $Å^{-1}$); (B) XANES; first-derivative absorption data in the pre-edge region are included as an inset. (a) 200 °C, data for the precursor have been included as dashed lines; (b) 400 °C; (c) 600 °C; (d) 800 °C.

Table 2. First-Shell Coordination Parameters Fitted to Fe K-Edge EXAFS[a]

T (°C)	*N*	$\Delta\sigma^2 \times 10^3$ (Å^2)	*R* (Å)	$\Delta E°$ (eV)
		ZAF−C-1		
original	6.0	6.6	1.99	7.0
200 °C	1.8	3.1	1.87	8.8
	3.3	3.0	2.02	5.8
400 °C	2.0	3.1	1.87	8.8
	3.2	2.4	2.02	4.6
600 °C	2.0	3.4	1.87	8.8
	3.1	2.6	2.02	5.0
800 °C	5.9	5.9	2.01	5.9
		ZA-F3		
400 °C	5.0	9.8	1.90	7.1
600 °C	5.9	7.1	1.99	3.0
800 °C	6.0	5.0	2.00	5.9

[a] Fit ranges: Δk = 3.2−12.8 $Å^{-1}$; ΔR = 0−2.2 Å. Estimated errors in coordination numbers (*N*) and shell radii (*R*) are ±10−15% and ±1−2%, respectively.

(30) An alternative model fits a single oxygen shell (for ZAF-C-1-600: N = 5.9; R = 1.97 Å; $\Delta\sigma^2$= 10.1 × 10^{-3} Å^2; $\Delta E°$ = 4.9 eV). Goodness of fit parameter for the single-shell model (ϵ_ν^2 = 17.1) is worse than calculated when two oxygen subshells are fitted (ϵ_ν^2 = 11.1), thus giving statistical significance to the latter model.

(31) Westre, T. E.; Kennepohl, P.; De Witt, J. G.; Hedman, B.; Hodgson, K. O.; Solomon, E. I. *J. Am. Chem. Soc.* **1997**, *119*, 6297.

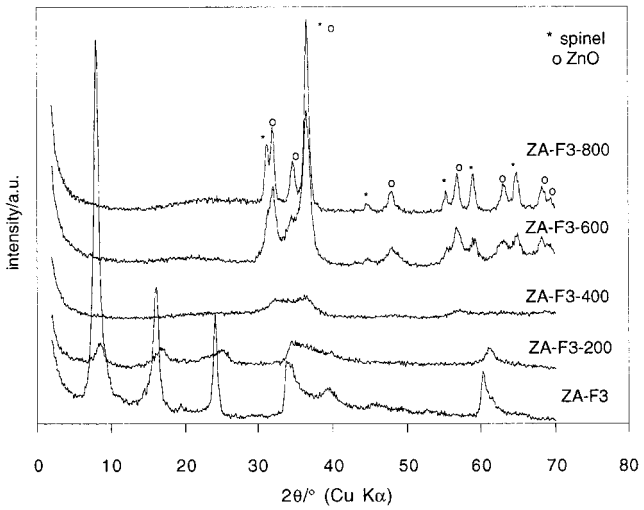

Figure 9. Powder X-ray diffraction patterns of ZA-F3-*T* samples. Patterns have been vertically displaced for clarity.

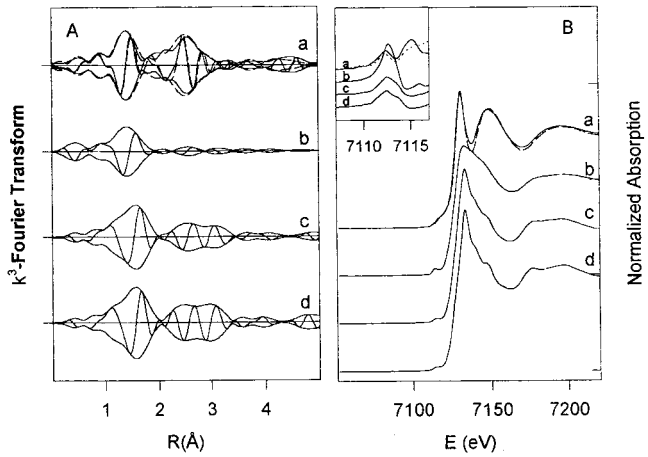

Figure 10. Fe K-edge XAS data for ZA-F3-*T*: (A) k^3-weighted Fourier transform of EXAFS oscillations ($\Delta k = 2.8-12.5$ Å^{-1}). (B) Fe K-XANES showing the first derivative of XANES data at the pre-edge region as an inset. (a) 200 °C, data for the precursor have been included as dashed lines; (b) 400 °C; (c) 600 °C; (d) 800 °C.

for all samples at the same position recorded for Fe$(NO_3)_3 \cdot 9H_2O$. Shifts to lower energies would be expected for Fe(II),[31] thus showing that iron is always as Fe(III) in these samples. Regarding the second-coordination shell of iron in ZAF-C-1-*T* samples, it splits into two overlapped maxima centered at 2.6 and 3.2 Å without phase shift correction. For ZAF-C-1-800 this result can be ascribed to the inclusion of Fe(III) cations in the spinel phase detected by PXRD. Fe(III) cations occupy octahedral holes in this sample. At the spinel structure, $[MO_6]$ octahedra share edges with other six octahedra and the vertex with six $[MO_4]$ tetrahedra. Fe−M distances determined from crystallographic data for Zn$Al_{2-y}Fe_yO_4$[29] are 2.9−3.0 Å for edge-sharing octahedra and 3.4−3.5 Å for vertex-sharing tetrahedron−octahedron pairs and, therefore, two distances separated by ca. 0.5 Å are expected at the second-coordination shell of iron. Although PXRD does not detect crystalline spinel phases in ZAF-C-*X*-*T* samples after calcination in the 200−600 °C range, the second-coordination shell of iron at these temperatures is nearly identical (see Figure 8A) to that recorded after calcination at 800 °C, only showing a lower intensity. This result shows that iron cations are included in a spinel-like phase in the amorphous materials obtained at intermediate calcination temperatures. Zn K-edge EXAFS data reported above showed that Zn−M distances characteristic of the spinel phases were absent at temperatures lower than 800 °C, thus suggesting that two different phases have segregated at 200−600 °C, one with a spinel-like structure including iron cations, probably amorphous γ-Fe_2O_3 with its deffective spinel structure,[23] and the second one with the ZnO structure including Zn cations.

PXRD data for the hexacyanoferrate sample (Figure 9) show a sharp decrease in the intensities of the diffraction peaks when the sample is calcined at 200 °C, thus indicating a loss of crystallinity. However, three weak harmonics at 10.38, 5.26, and 3.54 Å and a peak at 1.51 Å are still recorded and can be ascribed to diffraction by planes (003), (006), (009), and (110), respectively, of a material possessing the hydrotalcite structure. This means that a layered, but highly disordered, structure still exists, whose basal spacing is lower than that found in the starting material. Calcination at 400 °C collapses the layered structure. According to DTA data reported above, pyrolysis of the cyanide ligands has started at this temperature, and only a broad and ill-defined reflection extending from 2θ values of 32°−40° is recorded, indicating formation of a mostly amorphous material. When the sample is calcined at 600 °C, a temperature high enough to ensure complete pyrolysis of the cyanide ligands, crystallization of new phases has started, and diffraction peaks can be ascribed to a mixture of zincite and a spinel phase. After calcination at 800 °C, PXRD peaks ascribed to ZnO and spinel, already recorded at 600 °C, are sharper and better defined. New diffraction peaks are not recorded, and so changes in the 600−800 °C range correspond to an increase in the crystallinity of phases already formed at 600 °C.

XAS data at the Zn and Al K-edges for ZA-F3-*T* samples (not shown) are similar to those reported for ZAF-C-*X*-*T* samples. After calcination at 200 °C, Zn K-edge EXAFS show a low intensity of the second-shell maximum, but M−M shell radii are close to 3.0 Å, a value typical of the brucite-like layer. Only after calcination at a temperature equal to or higher than 400 °C first- and second-shell maxima appear at the positions characteristic of ZnO. Changes in zinc coordination when the calcination is increased (Figure 6C) are similar to those reported above for ZAF-C-1, although more stepwise, thus indicating a slower formation of the ZnO phase. On the other hand, and in agreement with PXRD data, the shoulder ascribed to the second-shell distances for Zn cations at the spinel phase appears already at 600 °C. As shown by an average Zn−O coordination number at the first shell close to 4, they occupy tetrahedral holes. Meanwhile, Al K-XANES for samples calcined at 200−600 °C show the low-energy shoulder at 1566 eV that disappears after thermal treatment at 800 °C. As discussed above for ZAF-C-*X*-*T* samples, this result again suggests for ZA-F3 the location at 200−600 °C of aluminum cations in tetrahedral oxygen coordination that migrate to octahedral holes after calcination at 800 °C.

Figure 10 includes data at the Fe K-edge for ZA-F3-*T* samples showing that after calcination at 200 °C, both

Fe K-edge EXAFS and XANES are nearly identical to those recorded for the precursor sample. Therefore, the structure of the hexacyanoferrate is maintained at this temperature and the lack of crystallinity detected by PXRD in ZA-F3-200 is due to a partial decomposition of the layer and not to destruction of interlayer species. Calcination at 400 °C leads to dramatic changes for Fe K-XAS data. Comparison of its associated FT (Figure 10A) with that recorded for the precursor shows that the first maximum broadens while the second maximum, ascribed to quasi-linear Fe−C−N chains, vanishes. Results indicate that hexacyanoferrate species are destroyed, leading to iron species in a highly disordered environment beyond the first-coordination shell. First-shell experimental data for this sample can be fitted (Table 2) with 5.0 Fe−O distances at 1.90 Å. A fit model similar to that obtained for ZAF-C-1-*T* ($200 \leq T \leq 600$ °C) and including two oxygen subshells at 1.87 and 2.02 Å, accounting for iron cations in tetrahedral and octahedral holes, respectively, was also tested. However, fit quality is not better than that obtained with the simplest fit model that considers a single Fe−O shell radii at 1.90 Å. Fe K-edge XANES for ZA-F3-400 (Figure 10B) shows broad features, the intensity of the pre-edge peak being higher than that recorded for the parent material, thus showing that, at least, some iron cations are in noncentrosymmetric coordination.[31] The presence of iron cations with a coordination number lower than 6, either in a square pyramidal coordination or as a mixture of species with tetrahedral and octahedral oxygen coordination, would account for the average coordination number at the first shell obtained from Fe K-edge EXAFS. A further increase of the calcination temperature leads to a lower intensity of pre-edge features, and Fe K-edge XANES for samples calcined at 600−800 °C are similar to that reported for $Fe(NO_3)_3 \cdot 9H_2O$.[8] Consequently, the intensity of the first-shell maximum at the FT associated with Fe K-edge EXAFS also increases. This maximum can be fitted by 5.9 oxygen atoms at 1.99 Å after calcination at 600 °C, while at 800 °C the best fit yields a single oxygen shell at 2.00 Å with a coordination number of 6.0. Results show that after calcination at a temperature high enough to decompose the hexacyanoferrate, at least a fraction of iron cations are in a coordination lower than six in an ill-crystallized oxygen framework, while most of them migrate to octahedral holes after calcination at 600 °C.

PXRD detected the formation of a spinel phase for ZA-F3-*T* samples already at 600 °C, whose crystallinity increased at 800 °C. As previously discussed for ZAF-C-1-800, the second-coordination shell of iron for ZA-F3-600 and ZA-F3-800 splits into two overlapped maxima, a result that was ascribed to the inclusion of Fe(III) cations in the spinel detected by PXRD. However, relative intensities of these maxima for ZA-F3-800 are clearly different from those recorded for ZAF-C-1-800. Because Fe and Al have different backscattering amplitudes, and Fe/Al atomic ratios are widely different for both materials (see Table 1), differences in the number of Fe and Al neighbors at the second shell may account for differences in the intensities of the second-shell maxima.

The Spinel Phases. XAS data indicate that Fe(III) and Al(III) occupy octahedral holes and Zn(II) tetrahedral holes at temperatures high enough to form a spinel that is detected by PXRD. As stated above, for $ZnAl_{2-y}Fe_yO_4$ normal spinels, [FeO_6] octahedra share edges with six other octahedra, yielding an Fe−M shell at 2.9−3.0 Å. This shell should include Fe and Al as backscatterers because both of them occupy octahedral holes in samples calcined at 800 °C. A longer Fe−M distance at 3.4−3.5 Å arises from [FeO_6] octahedra sharing a vertex with six tetrahedra, and because only Zn cations occupy tetrahedral holes in these samples, Zn backscatterers are expected at this distance. A determination of the Fe/Al ratio at 2.9−3.0 Å seems of interest because it would yield the average composition of the spinel phase where iron is included. To avoid ambiguities when fitting Fe and Al subshells, shell radii (R), Debye−Waller factors ($\Delta\sigma^2$), and inner potential corrections ($\Delta E°$) were constrained to be equal for both subshells. In the best fit to experimental data, R, $\Delta\sigma^2$, $\Delta E°$, the total coordination number, N, and the percentage of iron [Fe/(Fe + Al)] at ca. 3 Å were allowed to vary, together with coordination parameters (N, R, $\Delta\sigma^2$, $\Delta E°$) for the longer Fe−Zn shell. When working with a a k^3-weighting scheme (see Figure 11A), the fit to experimental data for ZA-F3-800 is optimized when the percentage of iron at ca. 3 Å is lower than 30%, while percentages of iron higher than 70% optimize the fit for ZAF-C-1-800. Therefore, fit results confirm that changes in the composition of the Fe/Al shell close to 3 Å are responsible for differences in the intensities of the maxima appearing at this distance. Moreover, because the dependence of k on the backscattering amplitude is different for low-Z (such as Al) and high-Z elements

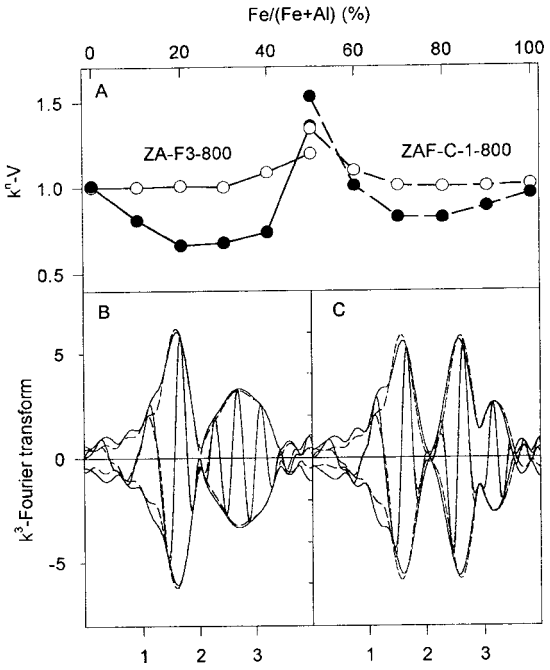

Figure 11. (A) k^n−V values[16] vs percentage of iron at 3 Å obtained through best fit to Fe K-edge EXAFS oscillations. Open and filled circles stand for values calculated using k^3- and k^0-weighted functions, respectively, while solid and dashed lines connect data obtained for ZA-F3-800 and ZAF-C-1-800, respectively. k^3-weighted Fourier transforms ($\Delta k = 3.2-12.8$ Å^{-1}) of experimental EXAFS oscillations (solid lines) and best fit functions (dashed lines) for (B) ZA-F3-800 (20% Fe at 2.93 Å) and (C) ZAF-C-1-800 (70% Fe at 2.97 Å). Coordination parameters are given in Table 3.

Table 3. Second-Shell Coordination Parameters Fitted to Fe K-Edge EXAFS for Samples Calcined at 800 °C[a]

shell	% Fe/(Fe + Al)	N	$\Delta\sigma^2 \times 10^3$ (Å^2)	R (Å)	$\Delta E°$ (eV)
		ZAF-C-1			
Fe/Al	70/80	6.0/5.3	5.1/5.4	2.97/2.97	10.0/10.0
Zn		3.7/3.1	8.7/7.5	3.46/3.47	10.0/8.9
		ZA-F3			
Fe/Al	20/30	5.6/6.9	3.4/2.9	2.93/2.97	0.7/−0.4
Zn		3.0/3.0	6.7/6.4	3.41/3.40	7.2/9.6

[a] Fit ranges: $\Delta k = 3.2-12.8$ Å^{-1}; $\Delta R = 0-4$ Å.

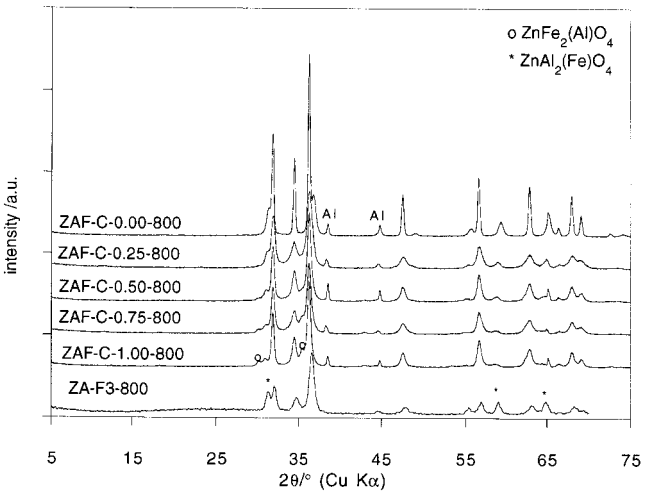

Figure 12. Powder X-ray diffraction patterns of samples calcined at 800 °C. Patterns have been vertically displaced for clarity. Diffraction peaks due to the Al sampleholder are marked.

(such as Fe), a comparison of the quality of the fit using the k^0-weighted function may help to distinguish Fe and Al as backscatterers,[32] and the iron percentage that optimizes both the k^0- and k^3-weighted fits was taken as the best value. As shown in Figure 11A, percentages of iron close to 20−30% and 70−80% form the second-coordination shell of iron for ZA-F3-800 and ZAF-C-1-800, respectively. Best fit parameters and functions are included, respectively, in Table 3 and Figure 11. Bulk Fe/(Fe + Al) atomic ratios for these samples (22% for ZA-F3 and 47% for ZAF-C-1) indicate that the second-coordination shell of iron has a composition close to that of the bulk material for ZA-F3-800, while it is enriched in iron for ZAF-C-1-800, thus showing a nonhomogeneous distribution of Fe^{3+} and Al^{3+} in the latter sample.

Information about the composition of the spinel phases can also be obtained from PXRD patterns recorded for samples calcined at 800 °C (Figure 12). For ZAF-C-0-800, where the only trivalent cation is aluminum, spinel diffraction lines can be ascribed to $ZnAl_2O_4$. As shown in Figure 12, peaks close to those expected for $ZnAl_2O_4$ are recorded in all samples prepared in the present study, but slightly shifted to higher d-spacing, thus suggesting that a fraction of Al^{3+} is substituted by the larger cation Fe^{3+}. Some of these peaks are overlapped with those corresponding to ZnO, so deconvolution has been made fitting the curve to a Pearson function. The value of the a parameter has been calculated from the positions due to diffraction by planes (220), (511), and (440), which are the peaks that appear

(32) Fung, A. S.; Kelley, M. J.; Koningsberger, D. C.; Gates, B. C. *J. Am. Chem. Soc.* **1997**, *119*, 5877.

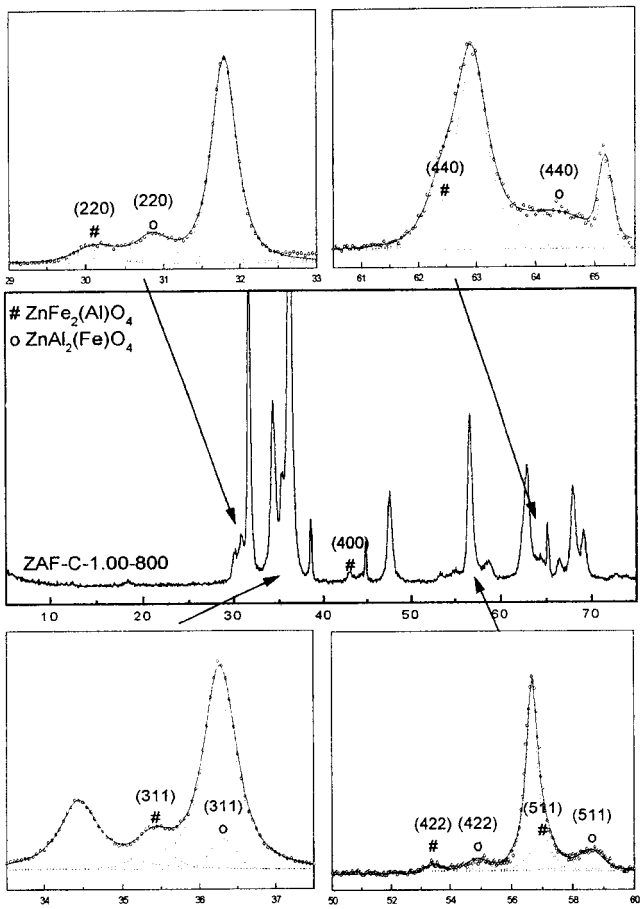

Figure 13. Powder X-ray diffraction pattern for ZAF-C-1-800 showing deconvolution results and ascription of diffraction lines to $ZnFe_2(Al)O_4$ and $ZnAl_2(Fe)O_4$ spinels (Open circles: experimental data; solid lines: best fit results; dotted lines: individual peaks).

in all the samples and with a tiny overlapping. From Fe/Al = 0.5 upward, a second set of diffraction lines, close to those expected for the spinel $ZnFe_2O_4$, is also recorded, although now slightly shifted to lower d-spacing, thus suggesting that a fraction of Fe^{3+} is substituted by the smaller Al^{3+}. In this case the a parameter was determined from the position of peaks due to planes (220), (311), and (400). The PXRD pattern corresponding to ZAF-C-1-800 is shown in Figure 13, where the different deconvolutions are also included and confirm the presence of two spinel phases, one aluminum-rich, $Zn[Al(Fe)]_2O_4$, and the other one iron-rich, $Zn[Fe(Al)]_2O_4$. According to XAS data, both spinels are essentially normal. Waerenborgh et al.[29] have reported a detailed study on cation distribution in synthetic $ZnFe_yAl_{2-y}O_4$ spinels ($0 \le y \le 2$) equilibrated at 1000 K, showing that all of them have a low inversion degree. These authors report a linear relationship between the Fe/Al ratio and the a parameter, and so, from a study of the precise positions of the PXRD peaks recorded, the composition of the spinels formed in our case can be concluded. Cell parameters (a) and degree of substitution (y, for $ZnFe_yAl_{2-y}O_4$) thus estimated are summarized in Table 4. For ZA-F3-800 a single spinel phase is formed, whose Fe/(Fe + Al) atomic ratio, 0.21, almost coincides with the value of the starting material, 0.22. For ZAF-C-X-800 samples, the aluminum-rich phase always has Fe/(Fe + Al) atomic ratios (0.10−0.28) that

Table 4. Cell Parameters and Composition of Aluminum-Rich and Iron-Rich Spinel Phases Detected in Samples Calcined at 800 °C

	$Zn[Al(Fe)]_2O_4$			$Zn[Fe(Al)]_2O_4$		
sample	*a* (Å)	*y*[a]	Fe/(Fe + Al)[a]	*a* (Å)	*y*[a]	Fe/(Fe + Al)[a]
ZAF-C-0.25	8.122	0.19	0.10			
ZAF-C-0.50	8.152	0.36	0.18	8.364	1.55	0.78
ZAF-C-0.75	8.171	0.47	0.23	8.389	1.70	0.85
ZAF-C-1.00	8.187	0.56	0.28	8.405	1.78	0.89
ZA-F3	8.160	0.41	0.21			

[a] Estimated values: *y* in $ZnAl_{2-y}Fe_yO_4$; Fe/(Fe + Al) atomic ratio.

are lower than the values for the starting materials (0.19−0.47), while for $X \geq 0.50$ a second spinel phase is detected, whose Fe/(Fe + Al) atomic ratio (0.78−0.89) is much higher than the corresponding value for the precursor. It should be noticed that homogeneous $ZnFe_yAl_{2-y}O_4$ spinels are in equilibrium at 730 °C, whatever the *y* value in the 0−2 range;[29] therefore, the segregation of two different spinels in our samples cannot be ascribed to thermodynamic effects. Experimental data suggested that ZnO and amorphous Fe_2O_3, the latter with a spinel-like structure, segregate after thermal treatments of the layered material at intermediate temperatures. Formation of two spinels at 800 °C suggest that an amorphous phase containing aluminum is also segregated at 200−600 °C. In the amorphous sample formed after calcining the precursor ZA-F3 at 400 °C, the spinel-like phase Fe_2O_3 was not detected, Fe K-edge EXAFS data showing a local environment of iron cations highly disordered beyond the first-coordination shell. These iron cations seem to be more reactive than those found in ZAF-C-*X*-*T* samples calcined at intermediate temperatures and react already at 600 °C to form a spinel with the same Fe/Al atomic ratio as the starting material. It seems that the higher reactivity of Fe(III) cations formed after pyrolysis of hexacyanoferrate(III) prevents the segregation of amorphous Fe_2O_3 and Al_2O_3 in this sample.

Acknowledgment. Authors thank for financial support CICYT (Madrid, Grants IN96-0252 and PB96-1307-C03), Junta de Andalucía (FQM214), and Daresbury Laboratories (UK, Grants 28/392 and 30/205).

CM0010856